AIAA Modeling and Simulation Technologies Conference
13 - 16 August 2012, Minneapolis, Minnesota

AIAA 2012-4717

# Integrated Simulation Models for High-Altitude Solar-Powered Aircraft

Andreas Klöckner*, Daniel Schlabe* and Gertjan Looye†
*German Aerospace Center (DLR), Oberpfaffenhofen, Germany*

**In recent years, there has been much research towards fixed-wing high-altitude solar-powered aircraft. Accurate knowledge about the behavior of the aircraft and its energy system is needed in order to plan and execute these aircrafts' missions. To this end, an integrated simulation model has been derived. It contains six-degrees-of-freedom flight dynamics, an energy system with solar cells, batteries, motors, and the effect of the environment on the solar radiation. A continuous day-and-night flight has been simulated and results are presented. The model represents all relevant effects for solar-powered aircraft including dynamic interaction between flight dynamics and energy system. The same model is used for pilot training and control design of the aircraft.**

## Nomenclature

*Abreviations*

| | |
|---|---|
| ELHASPA | Electric High-Altitude Solar-Powered Aircraft |
| 6DOF | Six degrees of freedom |
| WGS84 | World geodetic system |
| AVL | Athena Vortex Lattice |
| CAD | Computer Aided Design |
| AU | Astronomical unit |
| DC | Direct current |
| MC | Motor controller |
| BM | Battery management |
| SOC | State of charge |
| MPP(T) | Maximum power point (tracker) |

*Flight dynamics*

| | |
|---|---|
| $\alpha, \beta$ | Angles of attack and sideslip |
| $p, q, r$ | Rotational rates |
| $\delta_a, \delta_e, \delta_r$ | Aileron, elevator, rudder deflections |
| $C_L, C_D, C_Y$ | Force coefficients |
| $C_l, C_m, C_n$ | Moment coefficients |
| $m_a, I_a$ | Apparent mass and inertia |
| $\rho$ | Air density |
| $b, c$ | Surface strip's chord and width |

*Environment*

| | |
|---|---|
| $d$ | Time counted in days from 2000 |
| $N$ | Longitude of ascending node |
| $inc$ | Inclination to the ecliptic |
| $w$ | Argument of perihelion |
| $a$ | Semi-major axis |
| $e$ | Eccentricity |
| $M$ | Mean anomaly |
| $I_0$ | Solar constant |
| $I_d$ | Direct irradiance |
| $I_i$ | Diffuse irradiance |
| $I$ | Sensed irradiance |
| $h, z$ | True altitude and zenith angle |
| $h_a, z_a$ | Apparent altitude and zenith angle |
| $R$ | Atmospheric refraction |
| $AM$ | Relative air mass |

*Energy system*

| | |
|---|---|
| $i$ | Electric current |
| $v$ | Electric voltage |

*Research Assistant, Institute of Robotics and Mechatronics, Department of System Dynamics and Control, Münchner Straße 20, D-82234 Oberpfaffenhofen-Weßling.
†Senior Researcher, Institute of Robotics and Mechatronics, Department of System Dynamics and Control, Münchner Straße 20, D-82234 Oberpfaffenhofen-Weßling.

# I. Introduction

Solar-powered aircraft have received increasing interest by the scientific and industrial community in the past fifty years. The subject of early solar flight is summarized in depth by Boucher.[1] Voit-Nitschmann[2] and Noth[3] extend the overview and the latter also includes a list of flown solar aircraft with their basic characteristics. Recent developments of the Solar Impulse[4] and the QinetiQ Zephyr[5] prove that the technology is ready to allow for continuous solar-powered flight.

With the QinetiQ Zephyr at its lead, the research community also strives for unmanned solar-powered aircraft in high altitudes. The operation in high altitudes introduces several difficulties, summarized by Sobester[6] such that "any winged aircraft will inevitably be pushed to several of its limits simultaneously". This applies even more to solar-powered aircraft, which have very restricted power reserves and typically fragile light-weight structures.

This paper is related to the Electric High-Altitude Solar-Powered Aircraft (ELHASPA). It is developed and built by the German Aerospace Center's Robotics and Mechatronics Center in cooperation with several industrial partners and is intended to be used to advance technology and test applications for continuous high altitude solar flight. A picture of the aircraft is shown in Fig. 1.

**Figure 1. Elhaspa at its maiden flight**

Accurate knowledge about the behavior of the aircraft and its energy system in interaction with the environment is essential in order to plan and execute the aircraft's missions. In the context of automated mission management it is even more important to be able to rigorously analyse the aircraft's performance and to predict its trajectory. The first step towards these goals is a simulation model, which represents the relevant dynamic interactions.

In this paper an integrated approach to the simulation of flight dynamics, energy system and environment for a high-altitude, solar-powered aircraft is introduced. The three parts are driven by different fields of physical effects: mechanical, electrical, and atmospherical phenomena. Additionally, the parts interact in numerous and partly bidirectional ways as illustrated in Fig. 2.

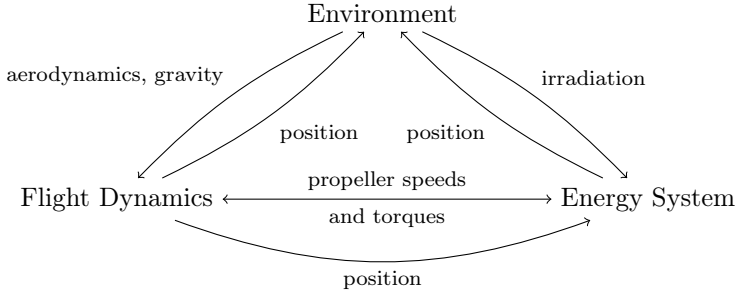


**Figure 2. Example of interactions between the model parts**

A modelling language specifically designed to cope with the dynamic simulation of multiple physical fields is Modelica.[7] It is also especially useful for bidirectional interactions, because it is an equation based modelling language and the simulation tool takes care of adequately solving the model equations. This also allows automated non-linear dynamic inversion of the models. The simulation described in this paper is implemented with the Modelica language.

The model is implemented in the framework of the Modelica Flight Dynamics Library.[8] The library already provides a great variety of basic aircraft models as well as environmental models necessary for six degrees of freedom (6DOF) and aeroelastic simulation of conventional aircraft. Positions can be expressed in the World Geodetic System (WGS84) and the rotation of the earth is taken into account. Detailled models of the magnetic and gravitational fields of the earth are included in the library as well as standard atmosphere data and wind simulation.

A major advantage of the Flight Dynamics Library is that it extensively uses standard Modelica mechanical connectors, such as MultiBody frames. This allows to connect any additional model with force or position interfaces to the airframe by a standardized interface without changing the inner model equations. Interactions other than mechanical connections are typically realized with Modelica's "outer" models providing global functions for the environmental properties. Busses are used for internal control signals. The present model makes use of these techniques and keeps up the interfacing philosophy.

In the following section, the integrated model structure (see Fig. 2) is explained and its three parts are detailled. The use of the model is demonstrated in the next section with the help of a day-night-cycle simulation. Finally, the lessons learnt so far and an outlook to future research is given.

## II. Simulation model

The interactions as illustrated in Fig. 2 are implemented in the Modelica language. This has been realized by the use of Modelica's outer models and Modelica's standard mechanical connectors, following the Flight Dynamics Library's interface philosophy.

The model consists of three parts: flight dynamics, energy system, and environment. The flight dynamics module contains the kinematic and force equations of the aircraft. It also contains models of actuators and sensors. The energy system module contains the model of the aircraft's power supply and eletrical loads. The environment modules contain reference systems, gravitation, wind, and atmospheric and solar effects.

The modularity of the library is maintained by defining additional modules and modular upgrades to existing modules. For example, the atmospheric effects on radiation are contained in a model called IrradianceUpgrade, which is then overloaded on the existing standard atmosphere model. The energy system is a completely new model and the modified flight dynamic modules can be seamlessly interchanged with the modules already provided by the Flight Dynamics Library.

Physical interactions between the modules are realized through standard interfaces. The position information is passed to the solar cell models through MultiBody frame connectors. This also allows to set separate locations and orientations for each solar panel.

The interaction between the energy system and the flight dynamics needs a bidirectional link through the propeller flange, because an equilibrium has to be maintained between the propeller and motor torques. This is realized with a standard Rotational Flange connector from the Modelica library.

The interactions with the environment modules are actually queries of the types: "How much solar radiation arrives at the current sensor position?" The environment is thus modelled with the use of outer models and their functions, which answer to exactly this kind of questions.

Command and sensor interfaces are realized with busses. The motor signals are rerouted through the motor model of the electric system instead of directly driving the engines.

The three parts of the integrated model are described in more detail in the following subsections.

### II.A. Flight Dynamics

The flight dynamics of the aircraft are governed by the three areas aerodynamics, weight-and-balance, and propulsion. Since they are represented through forces and motion, all modules can be expressed in separate models. They are then connected via MultiBody frames to the central airframe model, which implements the full 6DOF equations. Additional modules take care of the kinematic equations and input/output signals. Wheels are provided for simulating landing and take-off manoeuvres. The complete model structure is shown

in Fig. 3. Three new models have been developed: Aerodynamics, weight-and-balance, and propulsion. These modules are discussed in the following paragraphs.

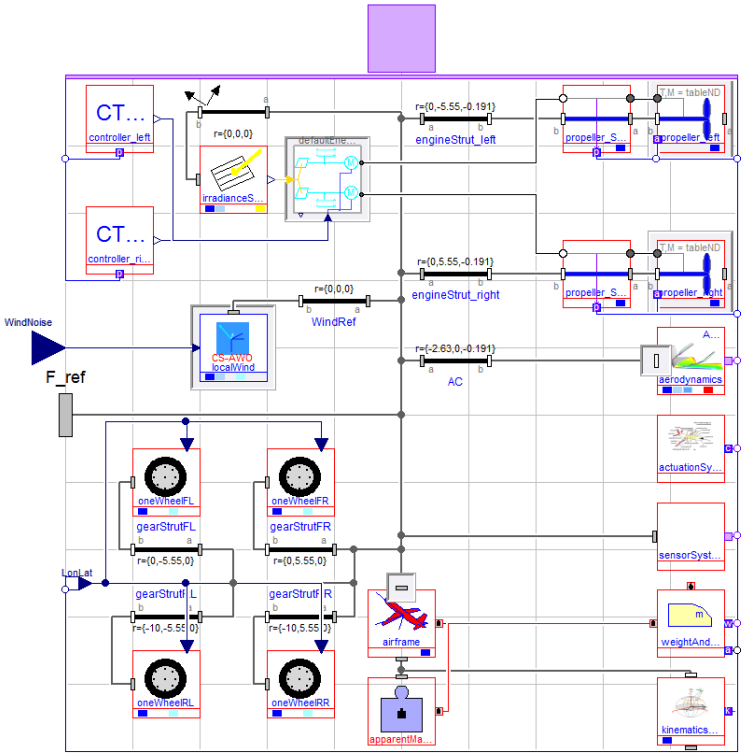


**Figure 3. A typical aircraft modelled with the Flight Dynamics Library**

The aerodynamics of the aircraft have been modelled using the Athena Vortex Lattice (AVL) software,[9] a potential flow simulation for thin airfoils. The model has been augmented with data obtained from Xfoil.[10] This program implements aerodynamic lift and drag estimations for two-dimensional airfoils. These routines provide fast aerodynamic estimations and they do not require extensive modelling. Thus, the aerodynamic methods described here were capable of easily following design changes and provided feedback to the design process in turn. Additionally, the test pilot reported similar behavior of the aircraft as compared to pilot trainings based on the simulation model.

The aerodynamic model is composed of the main wing, two horizontal, and two vertical stabilizers. It is depicted in Fig. 4 along with the AVL coordinate system. The model contains 1680 panels and six independently actuated control surfaces. All surfaces are augmented with Xfoil polars.

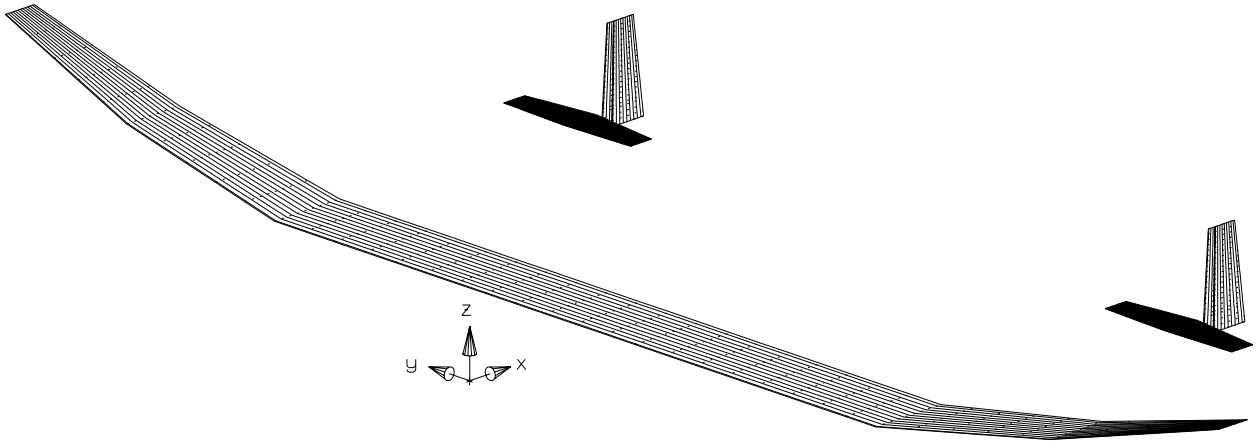


**Figure 4. Mesh of the aerodynamic model**

Since the computation of the flow field within AVL cannot be carried out in real time, the aerodynamic model was reduced to a polynomial approximation of the AVL model. To this end, a number of 10 000 points have been calculated in the relevant flight envelope. The resulting aerodynamic coefficients have been fitted in a least squares sense with multi-dimensional polynomials $\mathrm{p}(x_1, x_2, ...)$ in the aerodynamic angles ($\alpha$ and $\beta$), the rotational rates $(p, q, r)$ and the control surfaces $(\delta_a, \delta_e, \delta_r)$. These polynomials also cover coupling effects of the form $x_1^m \cdot x_2^n$. The output equations from the above procedure have the following form:

$$
\begin{aligned}
C_L &= \mathrm{p}\left(\alpha, q, \delta_a, \delta_e\right) && \text{(Lift coefficient)} \\
C_D &= \mathrm{p}\left(\alpha, q, \delta_a, \delta_e\right) && \text{(Drag coefficient)} \\
C_Y &= \mathrm{p}\left(\beta, p, r, \delta_a, \delta_r\right) && \text{(Side-force coefficient)} \\
C_l &= \mathrm{p}\left(\beta, p, r, \delta_a, \delta_e, \delta_r\right) && \text{(Rolling moment coefficient)} \\
C_m &= \mathrm{p}\left(\alpha, q, \delta_a, \delta_e\right) && \text{(Pitch moment coefficient)} \\
C_n &= \mathrm{p}\left(\beta, p, r, \delta_a, \delta_e, \delta_r\right) && \text{(Yaw moment coefficient)}
\end{aligned}
$$

AVL's coordinate and normalizing conventions differ slightly from the standard aeronautical conventions. An extension of the Flight Dynamics Library has thus been implemented, which provides all possible input and output variables to the aerodynamics' polynomials such as the output variables $C_l$ in body axes and $C_l'$ in stability axes. Thanks to Modelica's way of modelling, this leaves open, which of these variables is bound to the input variables through a polynomial, and makes a switch in variables a seamless operation.

The weight and balance of the aircraft has been estimated through a collection of mass points, which have been automatically extracted from a Computer Aided Design (CAD) model. During the building phases of the aircraft, the mass model has been updated continuously with new estimations and actual weights of the parts. For simulation purposes, the mass points are combined using the parallel axis theorem to form a single mass and inertia. Aeroelastic deformations are thus neglected for the current model state.

For a light-weight aircraft the apparent additional mass terms also turn out important: The mass of the dislocated air around the structure of the aircraft is in the same order of magnitude as the actual mass of the aircraft, adding up to considerably higher mass and inertia than estimated with the mere mass points. The apparent mass effect is estimated for small strips of the aerodynamics surfaces with a formula similar to the one given by Gracey.[11] The corrections are then combined in the same manner as the actual mass terms and applied to the airframe as an additional rigid body. The apparent mass actually depends on the air density, but it is assumed very slowly varying, such that the apparent mass module is assumed to have quasi-stationary mass properties. The estimation is given below as calculated in the AVL software:

$$
\begin{aligned}
m_{a,strip} &= \rho S \frac{\pi}{4} c \\
I_{a,strip} &= \rho S \frac{\pi}{4} c^3/64
\end{aligned}
$$

The aircraft is propelled by two propellers. Their characteristics have been estimated with the help of a Blade Element Method provided by the JavaProp software.[12] The resulting thrust force and the torque on the propeller shaft have been calculated for a grid of about 16 000 points at different propeller turn rates, aircraft airspeeds and altitudes. The propeller is driven through a Modelica standard rotational connector, which allows to connect arbitrary motor models to the propeller model, such as direct speed inputs or detailled motor models. The data is interpolated at runtime to yield the current propeller thrust and shaft torque. The resulting forces and moments are applied through a MultiBody connector to the airframe. An additional sensor model provides measurements of the propeller speed and thrust.

### II.B. Environment

The Flight Dynamics Library already provides an environment module, which keeps track of atmospherical quantities relevant to flight mechanics such as the wind, static pressure and air density, as well as gravity. It has been extended with additional components to simulate the position of the sun and the resulting solar irradiance as well as atmospheric refraction (ray deviation) and extinction (ray attenuation) of the solar radiation. This allows to simulate day/night cycles including a fine resolution at the horizon and attenuation of the solar radiation for altitudes close to the earth's surface.

The calculation of the sun's position has been derived from Modelica's Satellite Dynamics library, which implements interpolation in the International Astronomical Union's ephemerides files[13] as well as a simplified

analytical sun model by Schlyter.[14] This model implements the sun as a regular earth satellite on an elliptical orbit with the following orbital elements. In these equations, $d$ is the time counted in days of 24 h since the beginning of the year 2000.

$$\begin{aligned} N &= 0.0 && \text{(longitude of the ascending node)} \\ inc &= 0.0 && \text{(inclination to the ecliptic)} \\ w &= 282.9404 + 4.70935 \cdot 10^{-5} * d && \text{(argument of perihelion)} \\ a &= 1 \text{ AU} && \text{(semi-major axis)} \\ e &= 0.016709 - 1.151 \cdot 10^{-9} * d && \text{(eccentricity)} \\ M &= 356.0470 + 0.9856002585 * d && \text{(mean anomaly)} \end{aligned}$$

The sun's radiation can be assumed with a constant irradiance of $I_0 = 1366\ \mathrm{kW/m^2}$ or with an equivalent emmission, such that the irradiance varies with the distance between the sun and the earth and $I_0 = 1366\ \mathrm{kW/m^2}$ for a distance of 1 AU. The measured solar irradiance at the solar cell is further influenced by two atmospheric effects: refraction and extinction.

The atmospheric refraction $R$ deviates rays of the sunlight, such that the sun appears several arcminutes higher above the horizon than its actual location. These two positions are expressed as angles and are called apparent altitude $h_a$ and true altitude $h$ respectively. An accurate calculation of this effect requires numerical integration of the sunlight's path. An approximate calculation according to Saemundsson[15] has been implemented. It is reported to be accurate to 0.14 arcminutes for a standard atmosphere and locations at sea level:[16]

$$R = h_a - h \approx 1.02 \cot\left(h + \frac{10.3}{h + 5.11}\right).$$

The atmospheric extinction is expressed in terms of the relative air mass $AM$ located between the sensor and the sun. It is normalized such that for a sensor at sea level and the sun at the zenith the air mass is per definition 1. For sun positions close to the zenith the approximation for a plane-parallel atmosphere of $AM = 1/\cos(z)$ can be used. In this formula, $z = \pi/2 - h$ is the zenith angle between the zenith and the sun position. For positions closer to the horizon, interpolation formulas like the one developed by Young[17] need to be used. Young claims a maximum error of 0.0037 for the value of $AM$ at the horizon and for locations at sea level:

$$AM = \frac{1.002432\ \cos^2 z + 0.148386\ \cos z + 0.0096467}{\cos^3 z + 0.149864\ \cos^2 z + 0.0102963\ \cos z + 0.000303978}.$$

The actual direct irradiance $I_d$ arriving at a sensor is approximated for average air pollution and sea-level sensor locations by a formula given by Honsberg and Bowden.[18] Additionally, a fraction of 10 % of the direct irradiance is assumed to arrive at the sensor as diffuse (or indirect) irradiation $I_i$.

$$\begin{aligned} I_d &= I_0 \cdot 0.7^{AM^{0.678}} \\ I_i &= I_d \cdot 0.1 \end{aligned}$$

These formulas are valid for operation in relatively low altitudes. For actual stratospheric flight simulation, additional effects of the solar spectrum and modified extinction calculation have to be included in the models.

The irradiance $I$ sensed by the solar cell is then finally computed as the sum of the diffuse radiation and the direct radiation corrected by the angle between the apparent sun direction and the normal vector of the solar cell's surface:

$$I = I_i + I_d \cos \angle\left(normal, sun\right).$$

### II.C. Energy System

The energy system model computes the state of charge and available power of the solar cells taking into account efficiencies and losses of the system. In this way, one can assess the availability of power for different scenarios.

The top view of the electrical energy system model is shown in Fig. 5. The model consists of independent electrical systems for each side of the aircraft (i.e. left and right). Each side contains a solar energy generation block, a battery pack, an electric motor, and further technical loads. The batteries and the solar generation block are directly connected to the direct current (DC) main power bus. The motor is driven by a motor

controller (MC). The technical loads are powered by a DC/DC converter. A battery manager (BM) provides feedback on the current state of charge (SOC) to the solar energy generators. These components are described in the following.

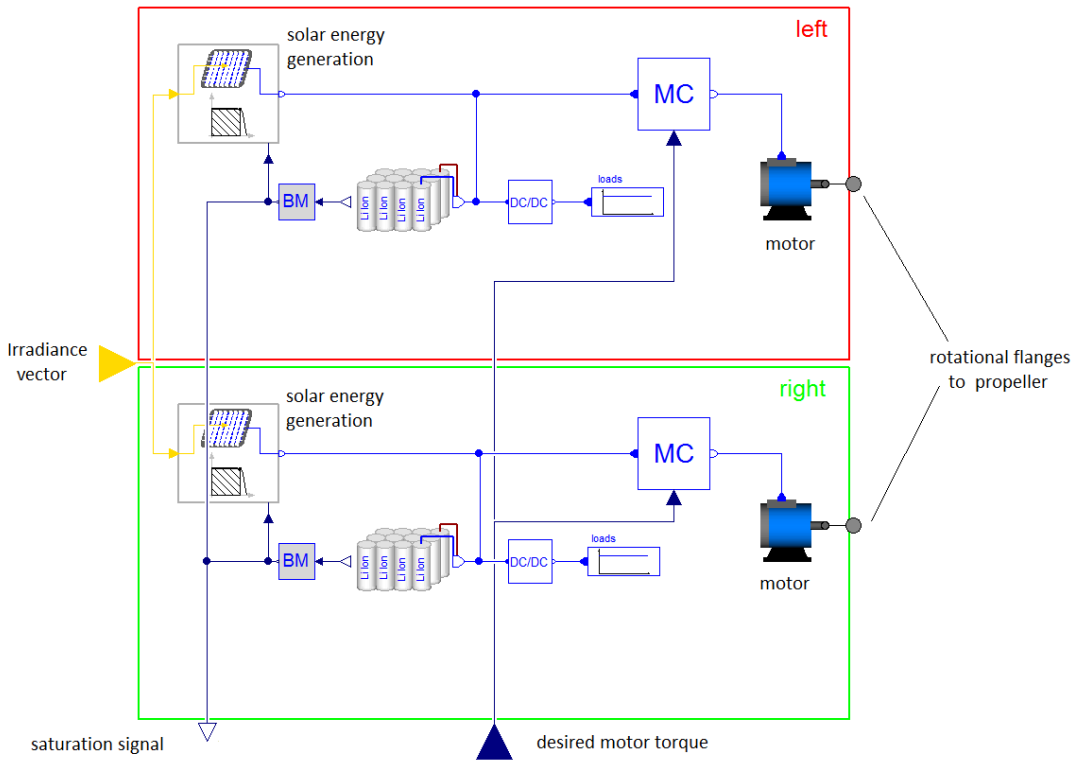


**Figure 5. Total model of the electrical energy system**

Each solar generation block contains several solar panels. Each solar panel has a dedicated position on the aircraft structure and thus is exposed to an individual irradiance. The sensed irradiance is computed with the procedure described in the previous subsection and fed to the individual solar panels. As a result, each panel generates its individual electrical power.

One solar panel is built up of several solar cells in series. The entire panel is modelled by means of one diode connected in parallel to a current source. The source generates a current proportional to the solar irradiance $I$. The dependency between electric current $i$ and voltage $v$ at the output connectors is thus described by

$$i = A \cdot I - B \cdot e^{v \cdot C}.$$

The parameters $A$, $B$, and $C$ of the solar panels have been derived from the solar cell datasheet. In power generating mode, a panel characteristic like in Fig. 6 is obtained for a fixed solar irradiance. The maximum power $i \cdot v$ is obtained in the so-called maximum power point (MPP). The MPP is also shown in Fig. 6. In order to always obtain the maximum power from a solar panel, its voltage is controlled by a DC/DC converter, called the maximum power point tracker (MPPT). The MPPT in this model uses the analytical derivative of the solar panel characteristics to set the panel voltage according to $\frac{\partial(i \cdot v)}{\partial v} = 0$. Actual MPPT would use observer approaches.[19] Since each solar panel can have a different orientation to the sun, each panel has its own power point tracker. All outputs of the maximum power point trackers are then connected in parallel to the main DC power bus.

The battery pack is modelled by a voltage source and an inner resistance. The values for voltage and resistance are variable and stored in look up tables as functions of the state of charge and current flow. The battery's state of charge is obtained by integrating the electric current. A battery manager (BM) is needed for controlling the current flow into the battery in order to prevent the battery from overload, since there is

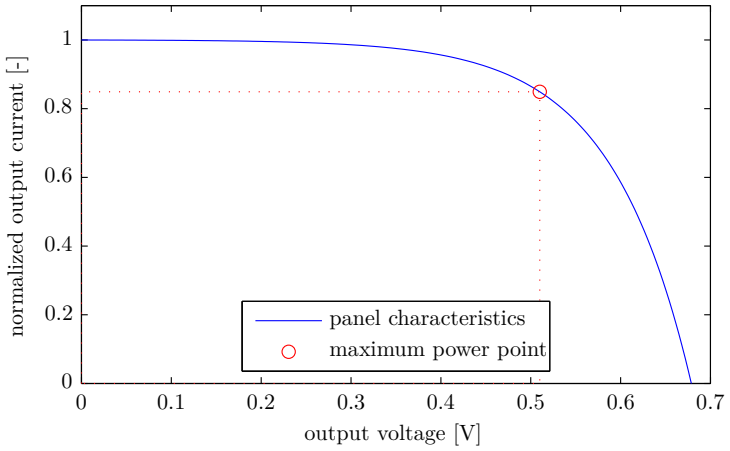


**Figure 6. Modelled characteristic of the solar cell and maximum power point**

no switch available to cut the battery from the electrical system. The BM measures the current SOC and compares it to $\mathrm{SOC}_{max}$, which is the maximum allowed SOC (e.g. 0.99). Then, a saturation signal *sat* is generated by the first PI-controller, which is added to the the input of the MPPT PI-controller as shown in Fig. 7. If *sat* is equal to zero (i.e. battery not fully loaded), the voltage of the respective solar panel $v$

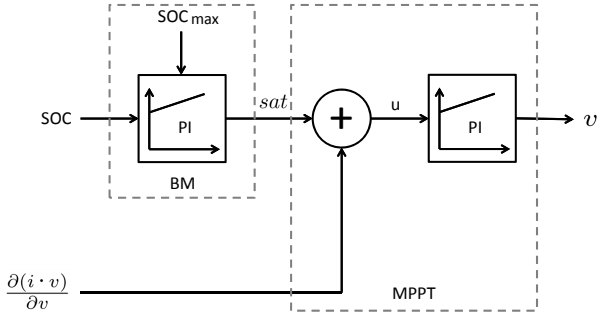


**Figure 7. Basic functionality of battery manager and power point tracker.**

is adjusted to achieve the maximum power output. That means the current flow at the MPPT output is maximized since its output voltage is nearly constant. If the maximum SOC has been reached, the saturation signal is unequal zero. Thus, the PI-controller of the MPPT will set a voltage $v$, which is not at maximum power point. The output current of the MPPT is reduced respectively. In that way, the current flow into the battery is controlled to be zero.

The electrical motor is the major consumer of electrical power and drives the aircraft propeller. The model consists of an electromagnetic force, which ideally transforms electrical energy into mechanical energy, an electrical resistor to consider copper losses, and a variable friction at the mechanical side to incorporate iron losses.

Technical loads like computers, servos, and communication devices are currently modelled by a fixed electrical resistance. These loads are powered by a DC/DC converter considering constant-efficiency as well as fixed losses of the converter.

Additionally to the interaction with the environment through the irradiance inputs, the energy system also interacts with the control system and the flight dynamics. The motor torques are commanded through a control signal. The internal saturation signal is provided for use in the control loops. It indicates the amount of currently unused solar power. Finally, a Modelica rotational flange is provided for connection with the propeller shaft driving the propeller of the flight dynamics.

## III. Results

In this section, the results obtained with the model are described briefly for a day-and-night flight at a location close to the equator and starting in the morning of July 1st 2012. A non-linear inverted model has been used for the simulations similar to the one described by Mueller.[20] It is driven by the flight path inputs calibrated airspeed, altitude and track angle and is thus independent of the controller design. All regular inputs such as motor commands are automatically derived from the flight path inputs.

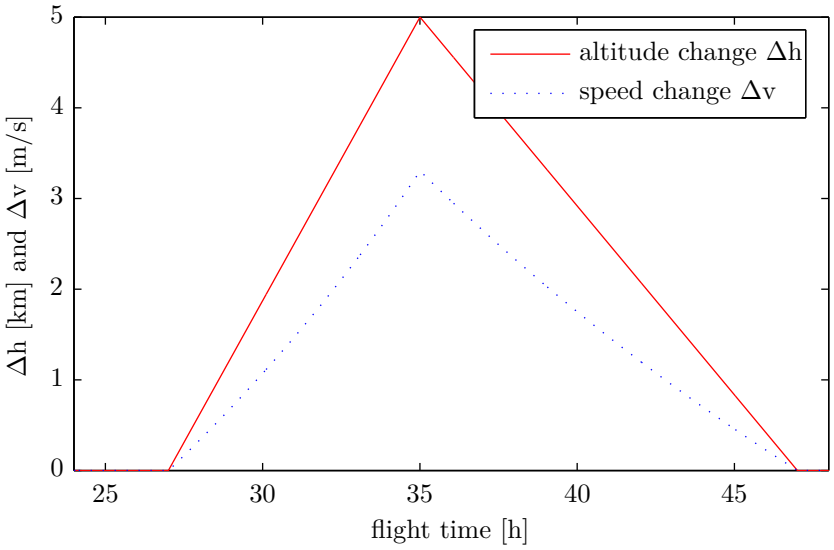


**Figure 8. Aircraft altitude and velocity during a full day's flight**

Figure 8 shows the energetically relevant variables of the aircraft's flight path for 24 h starting from sunrise. During the day, the aircraft develops a constant climb rate. The additional altitude is decreased continuously during the night in order to reduce the energy required by the motor. The aircraft actually flies with constant calibrated airspeed, such that the true airspeed is adjusted to the altitude.

In Fig. 9 the solar and atmospheric variables are plotted during daytime. The apparent altitude of the sun indicates sunrise and sunset at its zero-crossings. Close to the horizon the atmospheric refraction is quite important and leads to a slightly longer day-time compared to calculations with the true altitude. Also the relative air mass is very important near the horizon. This causes strong atmospheric extinction in early and late day times.

The extinction effect can be seen in Fig. 10. It shows the irradiance recorded during daytime. The irradiance arriving at the outer atmosphere of the earth is assumed constant with 1366 $W/m^2$. It is extinguished by the important air mass to nearly zero during sunrise and sunset. Also at noon, only a total irradiance of about 1000 $W/m^2$ arrives at the sensor. This includes direct and diffuse irradiance. The plot also shows the sensed irradiance values for three solar arrays. The leftmost solar arrays have been tilted slightly to the right in order to simulate the wing's dihedral. The corresponding rightmost arrays have been tilted to the left in the same amount. A middle solar array is plotted for comparison. The different irradiances for both panels can be seen in the plot.

Figure 10 additionally shows the coupling between the flight dynamics and the irradiance received by the solar panels. In the second half of the day the aircraft prescribes a turn of 180°, which causes important changes in the sensed irradiance.

The different irradiances also cause different charge states of the batteries. In Fig. 11, the state of charge of a left battery is compared against the state of charge of a right battery for the complete flight. Both batteries start with a charge of 80 %. Their states of charge diverge during the day. This effect is caused by the different installation angles of the solar panels. Both batteries can be fully recharged during daytime in this advantageous scenario. In different locations, less power is available.

The resulting power output of the left side's electrical modules is shown in Fig. 12. While charging the

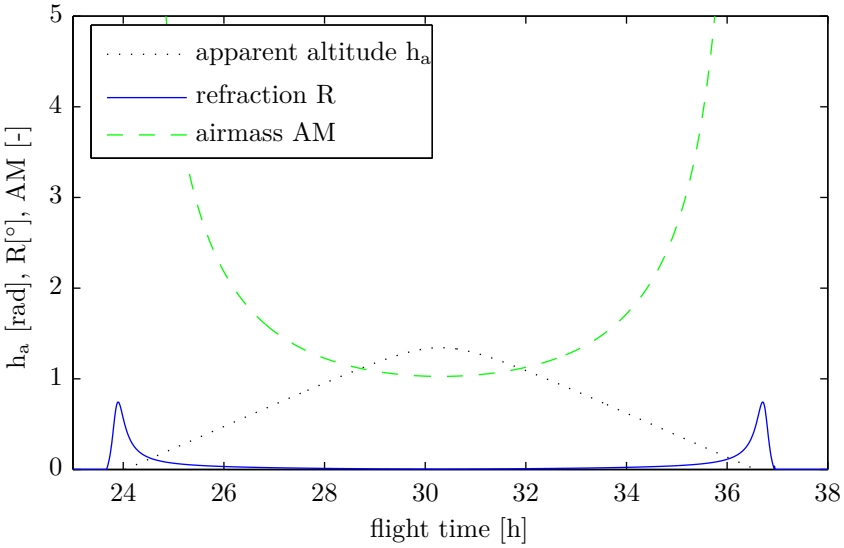


**Figure 9. Solar and atmospheric variables during daytime**

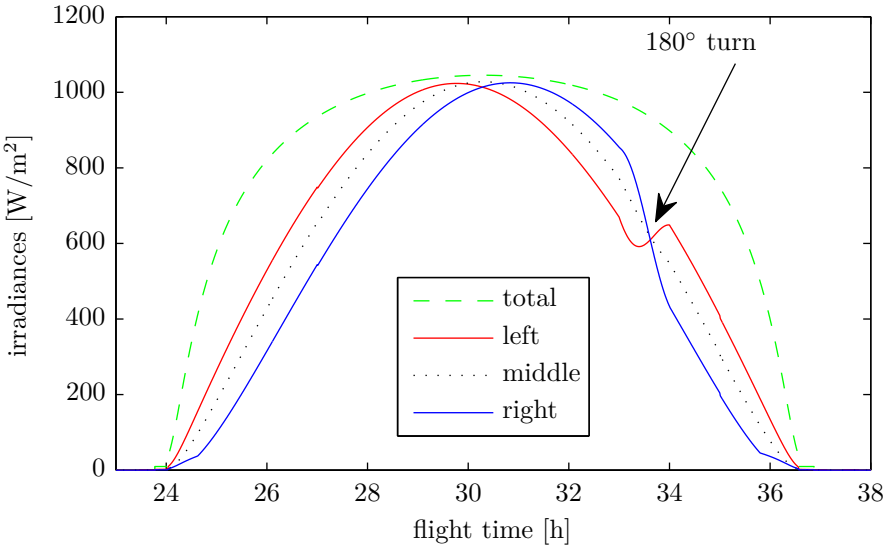


**Figure 10. Irradiance during daytime onto solar panels with different orientation**

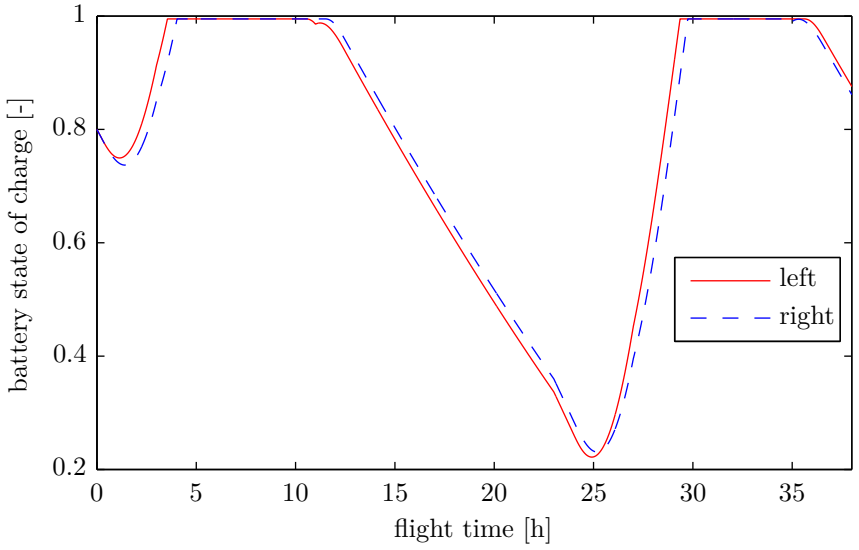


**Figure 11. Battery state of charge for two batteries for the complete flight**

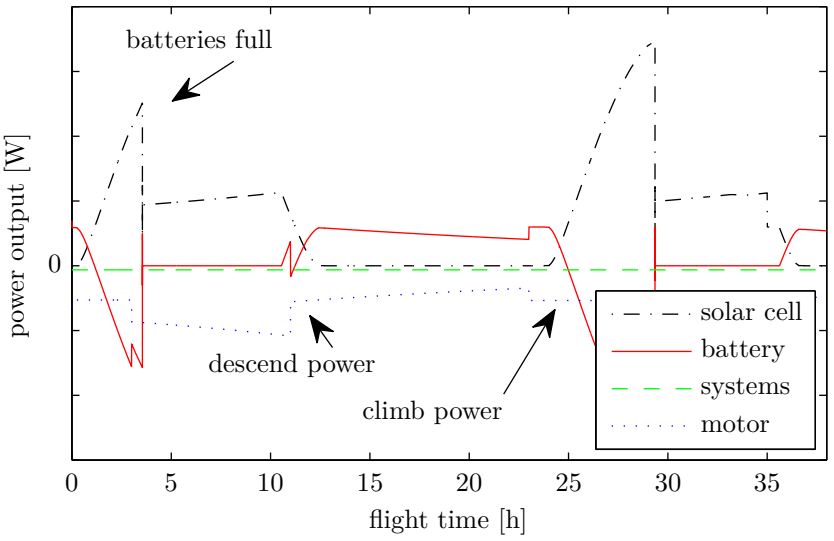


**Figure 12. Power output of the energy system components for the complete flight**

battery at the beginning of the simulation, the solar arrays' power output is a function of the irradiance value. This is due to the maximum power point tracker, which maintains the maximum power point of the cells. It powers the motor and the systems and charges the battery at the same time.

When the batteries are fully recharged, the battery management decreases the solar cell's output power in order to not damage the batteries. During descend in the night, a decreased power consumption of the motor can be noticed. The solar cells do not generate power and the aircraft is now powered by the batteries. When the motor is switched on in the morning, the cycle starts over. The changing motor power consumption in steady climb and descend is caused by the changing air density and flight velocity.

## IV. Conclusion and Outlook

We have presented an integrated simulation model of a high-altitude solar-powered aircraft. The model contains a comprehensive simulation of all relevant effects for solar-powered aircraft and their energy systems. The model represents dynamic interactions between the energy system and the flight dynamics as well as environmental effects. In addition, the model is inverted automatically for a mission simulation.

Results of an exemplary day/night cycle simulation have been presented. The results promise a deeper insight in the problems of operating such aircraft. Especially, it is indecated that a sophisticated energy and mission management must be implemented in order to achieve continuous flight during more than one day.

Future research and development will steer towards enhancement and validation of the models. The aerodynamic modelling process will be validated for use with different aircraft and the flight mechanics model will be validated and updated with flight test data. Ground and flight tests will be used to validate the electric system model. The overall flight performance will be compared between simulation and actual flight data.

The model will be extended with electric models of the relevant systems. Especially the servos and their varying energy consumption will be taken into account. This will also introduce further coupling through the control surfaces' hinge moments. The environment models will be extended for use in higher altitudes. Aeroelastics and instationary aerodynamics will be included using the method of Kier et al.[21] Additionally, the use of external software will be decreased in the generation of future model updates.

Other future research directions will make use of the developed model for pilot and operator training, autopilot development and as a mission and operation planning tool. Special emphasis will be put on the development of automatic mission management routines, which will make extensive use of the integrated simulation model.

## References


[1]Boucher, R., "History of solar flight," *AIAA paper*, 1984, pp. 84–1429.

[2]Voit-Nitschmann, R., "Solar- und Elektroflugzeuge – Geschichte und Zukunft," *Jahrbuch aus Lehre und Forschung der Universität Stuttgart*, Universität Stuttgart, 2001, pp. 88–99.

[3]Noth, A., "History of Solar Flight," Aircraft & spacecraft systems design lecture notes, Autonomous Systems Lab, ETH Zürich, Switzerland, 2008.

[4]Solar Impulse, S., "Solar Impulse – Around the world in a solar airplane," online at `http://solarimpulse.com/`, 2011.

[5]QinetiQ Group, PLC, "Zephyr UAV," online at `http://www2.qinetiq.com/home_farnborough_airshow/unmanned_air_systems/zephyr.html`, 2010.

[6]Sobester, A., *Stratospheric Flight: Aeronautics at the Limit*, Springer-Praxis, 2011.

[7]Fritzson, P., *Principles of object-oriented modeling and simulation with Modelica 2.1*, Wiley-IEEE Press, 2004.

[8]Looye, G., "The new DLR flight dynamics library," *Proceedings of the 6th International Modelica Conference*, Vol. 1, 2008, pp. 193–202.

[9]Drela, M. and Youngren, H., "Athena Vortex Lattice," online at `http://raphael.mit.edu/avl`, September 2004.

[10]Drela, M. and Youngren, H., "Xfoil – Subsonic Airfoil Development System," online at `http://raphael.mit.edu/xfoil`, April 2008.

[11]Gracey, W., *The Additional-Mass Effect of Plates as Determined by Experiments*, National Advisory Committee for Aeronautics, 1941.

[12]Hepperle, M., *JavaProp Users Guide*, November 2010.

[13]International Astronomical Union, "Ephemerides," online at `http://iau-comm4.jpl.nasa.gov/`, 2010.

[14]Schlyter, P., "How to compute planetary positions," online at `http://stjarnhimlen.se/comp/ppcomp.html`, 2011.

[15]Saemundsson, T., "Atmospheric Refraction," *Sky And Telescope*, Vol. 72, July 1986, pp. 70.

[16]Meeus, J., *Astronomical algorithms*, Willmann-Bell, Incorporated, 1991.

[17]Young, A. T., "Air Mass and Refraction," *Applied optics*, Vol. 33, No. 6, 1994, pp. 1108–1110.

[18]Honsberg, C. and Bowden, S., "PVCDROM," online at `http://www.pveducation.org/pvcdrom/properties-of-sunlight/air-mass`, 2010.

[19]Hohm, D. and Ropp, M., "Comparative study of maximum power point tracking algorithms," *Progress in photovoltaics: Research and Applications*, Vol. 11, No. 1, 2003, pp. 47–62.

[20]Mueller, R., "Multi-objective optimization of an aircraft trajectory betweeen cities using an inverse model approach," *AIAA Modeling and Simulation Technologies Conference*, (to be published), 2012.

[21]Kier, T., Looye, G., Scharpenberg, M., and Reijerkerk, M., "Process, methods and tools for flexible aircraft flight dynamics model integration," *International Forum on Aeroelasticity and Structural Dynamics*, Stockholm (Schweden), 2007.